2-^{18}F-Fluoropropionic Acid as a PET Imaging Agent for Prostate Cancer

NagaVaraKishore Pillarsetty, Blesida Punzalan, and Steven M. Larson

Department of Radiology, Memorial Sloan-Kettering Cancer Center, New York, New York

There is a high interest in developing an ^{18}F-labeled PET tracer that can aid in diagnosis and therapy monitoring of prostate cancer. In the current study, we have evaluated the potential of 2-^{18}F-fluoropropionic acid (^{18}F-FPA) as a PET tracer for imaging prostate cancer. **Methods:** ^{18}F-FPA was synthesized starting from methyl-2-bromopropionate. Small-animal PET studies were performed on mice with CWR22rv1, PC-3, DU-145, and LNCaP prostate xenografts, and comparison of imaging characteristics of ^{18}F-FPA with ^{18}F-FDG uptake is reported. Biodistribution studies with ^{18}F-FPA were performed on mice with CWR22rv1 xenografts and compared with ^{14}C-acetate. **Results:** ^{18}F-FPA was synthesized in 44% overall radiochemical yield (decay-corrected). Small-animal PET studies revealed that ^{18}F-FPA can delineate both androgen-dependent and androgen-independent prostate xenografts with high tumor-to-background ratios. Comparative imaging studies demonstrate the superior performance of ^{18}F-FPA over ^{18}F-FDG for imaging prostate cancer, with excellent tumor-to-background contrast. Biodistribution studies show that tumor uptake of the tracer was 5.52 ± 0.35, 5.53 ± 0.42, 5.74 ± 0.54, and 5.34 ± 0.19 percentage injected dose (%ID) per gram at 1, 2, 3, and 4 h, respectively, after injection. The %ID/g values for ^{18}F-FPA and ^{14}C-acetate 1 h after tail vein injection were 7.08 ± 0.80 and 0.36 ± 0.08 in tumor, and the corresponding tumor-to-muscle ratios were 1.94 and 2.06, respectively. **Conclusion:** The data presented here indicate that ^{18}F-FPA accumulates in prostate cancers with high tumor-to-background ratios. ^{18}F-FPA has potential for use in the clinical diagnosis of prostate cancer in humans.

Key Words: prostate cancer; PET; ^{11}C-acetate; 2-^{18}F-fluoropropionic acid; CWR22rv1

Prostate cancer is the most commonly diagnosed and second leading cause of cancer deaths in men in the United States (*1*). If detected early, prostate cancer treatment is highly successful, but at present there are no known treatments for advanced metastatic disease. For primary prostate tumors, determining the precise location and defining the target are critical for defining the clinical target volume for conformal radiotherapy (*2*). The field of noninvasive molecular imaging using PET isotopes has made rapid advances for the detection of primary and metastatic tumors, with ^{18}F-FDG leading the way as a universal tumor-imaging agent. However, for prostate cancer, the results with ^{18}F-FDG have been suboptimal (*3*). Hence, there is an urgent need to develop PET agents that can be used for routine detection and characterization of prostate tumors. Both ^{11}C- and ^{18}F-labeled radiotracers have been developed, including ^{11}C-acetate, ^{11}C-choline, ^{18}F-fluoroacetate (*4,5*), and ^{18}F-fluoroethylcholine (*6–9*), among others. ^{11}C-acetate has shown promising results for the diagnosis of primary and metastatic prostate cancer, but the short half-life of ^{11}C (20 min) means that ^{11}C tracers can be used only at facilities that have an on-site cyclotron. ^{11}C is impractical for use as a routine PET tracer in many imaging centers. ^{18}F-labeled agents offer practical benefits due to a relatively long half-life (110 min). In this regard, ^{18}F-fluoroacetate (*4,5*) and ^{18}F-fluorine derivatives of choline (*6–9*) are currently being investigated as prostate tumor–imaging agents. ^{18}F-fluoroacetate is a substrate for acetyl coenzyme A synthase and hence mimics ^{11}C-acetate in the primary steps and has been proposed as a useful alternative for prostate cancer imaging. ^{18}F-fluoroethylcholine mimics choline that is trapped inside the cells after phosphorylation by choline kinase, which is overexpressed in tumor cells. So far, no clear winner has emerged for prostate cancer.

In our continuing effort to identify novel PET tracers for oncologic applications (*10–13*), we have identified 2-^{18}F-fluoropropionic acid (^{18}F-FPA) as a possible radiotracer for imaging prostate cancer. The hypothesis is that ^{18}F-FPA would mimic acetate in vivo in the same way that fluoroacetate mimics acetate (*14,15*) and hence would accumulate in prostate cancer and allow tumor delineation by PET. In support of this hypothesis, we present preliminary data including biodistribution and PET studies with ^{18}F-FPA. The results suggest the potential use of ^{18}F-FPA as a new PET radiotracer for imaging prostate cancer and provide a rationale for further laboratory and clinical characterization of this tracer.

MATERIALS AND METHODS

All reagents and solvents were purchased from either Aldrich Chemical Co. or Fisher Scientific and, unless stated otherwise, were used without further purification. All high-performance

liquid chromatography (HPLC) solvents were filtered (0.45 μm, nylon, Alltech) before use. Water (ultrapure, ion-free, >18.2 MΩ · cm^{-1}) was obtained from a Millipore α-Q Ultra-pure water system. HPLC was performed using a Shimadzu system equipped with a C-18 reversed-phase column (Phenomenex Luna analytic 4.6 × 250 mm or SemiPrep 21.2 × 100 mm, 5 μm, 1.0 or 6.0 mL/min, 0.2% acetic acid/CH$_3$CN), 2 LC-10AT pumps, an SPD-M10AVP photodiode array detector, and a BioScan Flow Count *PIN* diode radiodetector. Radioactivity was assayed using a Capintec CRC-15R dose calibrator.

No-carrier-added ^{18}F-fluoride ion was produced by the ^{18}O$(p,n)^{18}$F nuclear reaction by bombardment of an enriched ^{18}O-H$_2$O target with 11-MeV protons using an EBCO TR-19/9 cyclotron.

Synthesis of ^{18}F-FPA

^{18}F-FPA was synthesized using an established procedure (Scheme 1) (*16*). Briefly, ^{18}F-fluoride ion (2.8 GBq = 75 mCi) in water was added to a vial containing 80 μL of 0.25 M potassium carbonate and 13 mg of Kryptofix dissolved in 1 mL of acetonitrile. Water was removed azeotropically with acetonitrile (3 × 1 mL) at 80°C. To the anhydrous ^{18}F-KF/K$_2$CO$_3$ complexed with Kryptofix was added a solution of methyl-2-D,L-bromopropionate (3 mg) in 300 μL of anhydrous acetonitrile, and the vial was sealed and heated at 80°C for 6 min to give methyl-2-^{18}F-fluoropropionate. The vial was allowed to cool to room temperature and diluted with 700 μL of water and purified using HPLC. The intermediate was purified on a semipreparative Phenomenex reversed-phase C-18 column (Gemini-NX, 100 × 21.2 mm, 5 μm, 110 A) using a mixture of 0.2% aqueous acetic acid:acetonitrile (60:40) as the eluant, with a flow rate of 6 mL/min. The product methyl-2-^{18}F-fluoropropionate, with a retention time of 5.4 min, was collected. To the product, 50 μL of 10N sodium hydroxide was added and heated at 80°C for 10 min to give sodium 2-^{18}F-fluoropropionate. The solvent was removed under reduced pressure, and the residue was neutralized with 85 μL of 6N HCl. The product was formulated in 0.9% saline and used for studies. For analysis of purity, 40 μL of product were acidified with 10 μL of 10N HCl and passed through a reversed-phase C-18 column (Luna, 250 × 4.6 mm, 5 μ, 100 A) using 0.2% aqueous acetic acid as the eluting solvent, with a flow rate of 1 mL/min. The final radiochemical yield was around 44% ± 3% (nonoptimized), with a specific activity of around 50 GBq/μM.

Octanol–Water Partition Coefficient Study (logP)

Octanol–water partition coefficients were determined for ^{18}F-FPA at 4 different pH values—6.4, 7.0, 7.4, and 8.4—by measuring the distribution of radiolabeled compound in 1-octanol and phosphate-buffered saline. A 20 μL sample of ^{18}F-FPA (~10–20 μCi) in saline was added to a vial containing 5 mL each of 1-octanol and phosphate-buffered saline. After being stirred in a vortex mixer for 1 min, the vial was centrifuged for 5 min to ensure complete separation of layers. Five hundred microliters of each layer were

taken in a preweighed vial, and ^{18}F counts (400- to 550-keV energy range) were measured using a γ-counter (PerkinElmer 1480 Wizard 3 Auto γ-counter). Counts per unit weight of sample were calculated, and logP values were calculated using the following formula:

$$\log_{10}P = \log_{10}(\text{counts in 1 mL of octanol/counts in 1 mL of water}).$$

Generation of Tumor Xenografts

All animal experiments were conducted in accordance with protocols approved by the Institutional Animal Care and Use Committee of Memorial Sloan-Kettering Cancer Center and followed National Institutes of Health guidelines for animal welfare. Tumor cell lines were obtained from the American Type Culture Collection and cultured under conditions provided by the supplier. The cell lines included CWR22rv1, PC-3, LNCaP, and DU-145. Subcutaneous tumors were produced in nude mice (20–25 g; Taconic) by subcutaneous injection of 5 × 10^6 tumor cells in 200 μL consisting of 100 μL of cell culture medium and 100 μL of Matrigel (BD Biosciences) under 2% isoflurane anesthesia on the right forelimb of mice.

Small-Animal PET

Imaging was performed by use of a dedicated small-animal PET scanner (Focus 120 microPET; Siemens Medical Solutions USA, Inc.). The mice were maintained under 2% isoflurane anesthesia in oxygen at 2 L/min during the entire scanning period. Imaging was performed 1 h after administration of 11.1 MBq (300 μCi) of either ^{18}F-FPA or ^{18}F-FDG via injection in the tail vein. For a comparative study, mice were kept fasting for 4 h and imaged with ^{18}F-FDG 1 h after intravenous injection. The activity was allowed to decay for 24 h, and then the mice were administered ^{18}F-FPA via the tail vein and imaged 1 h after injection. An energy window of 350–700 keV and a coincidence timing window of 6 ns were used. The image data were corrected for nonuniformity of the scanner response, dead-time count losses, and physical decay to the time of injection. No correction was applied for attenuation, scatter, or partial-volume averaging. The measured reconstructed spatial resolution of the Focus 120 scanner is approximately 1.6 mm in full width at half maximum at the center of the field of view. The counting rates in the reconstructed images were converted to activity concentrations (percentage injected dose [%ID] per gram of tissue) by use of a system calibration factor derived from the imaging of a mouse-sized water-equivalent phantom containing ^{18}F.

In Vivo Biodistribution Studies

For single-isotope (^{18}F) biodistribution studies, mice with CWR22rv1 tumors were injected in the tail vein with 3.7–5.5 MBq (100–150 μCi) of ^{18}F-FPA in 200 μL of saline. Radioactivity in the syringe before and after administration was measured in an energy-calibrated dose calibrator (CRC-15R), and the exact quantity received by each animal was determined. The animals were euthanized at different time points, and then the organs
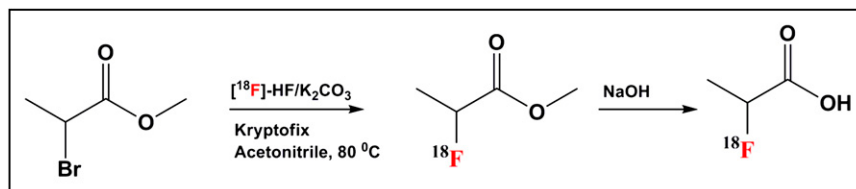
SCHEME 1. Synthesis of ^{18}F-FPA.

were harvested. ^{18}F radioactivity was measured in a calibrated γ-counter (1480 Wizard 3 Auto γ-counter) using a 400- to 600-keV energy window and decay correction. The counts were converted into activity, and %ID/g was calculated by dividing by decay-corrected injected activity and weight of the organ. For dual-isotope biodistribution studies, each animal was administered 200 μL of saline containing 3.7 MBq of ^{18}F-FPA and about 0.0037 MBq (0.1 μCi) of ^{14}C-acetate. Initially, ^{18}F radioactivity was measured in a calibrated γ-counter (1480 Wizard 3 Auto γ-counter) using a 400- to 600-keV energy window and decay correction. For measuring ^{14}C activity, all samples were solubilized (Soluene-350, Packard Instrument Co., Inc.) after the ^{18}F radioactivity counting. The samples were then stored at 4°C for 1 d to allow for ^{18}F decay. A scintillant agent (Insta-Fluor; Packard Instrument Co., Inc.) was added to solubilized samples, and ^{14}C radioactivity was determined by liquid scintillation counting (Tri-Carb Liquid Scintillation Analyzer, model 1600TR; Packard Instrument Co., Inc.) using external standard quench corrections. The counts were converted into activity, and %ID/g was calculated by dividing by decay-corrected injected activity and the weight of the organ. For each time point, a minimum of 3 animals was used for the study, and the values are reported as mean ± SD of mean. The Student t test was performed, and differences were considered statistically significant at $P < 0.05$.

RESULTS

Synthesis

The overall synthesis time for ^{18}F-FPA was 45 min, and the average radiochemical yields were about 44% ± 3% (decay-corrected). The radiochemical purity was at least 98%. The average specific activity was 50 GBq/μM.

Octanol–Water Partition Coefficient Study (logP)

Lipophilicity logP values of ^{18}F-FPA at pH 6.4, 7.0, 7.4, and 8.4 are −2.89 ± 0.02, −3.08 ± 0.04, −2.97 ± 0.13, and −3.07 ± 0.03, respectively. As expected, for small carboxylic acids the logP is very low, indicating that the compound is very hydrophilic. The lipophilicity is not sensitive to changes in pH within the measured physiologically relevant pH ranges.

Small-Animal PET

Small-animal PET was performed to evaluate the potential of ^{18}F-FPA as a tumor-imaging agent in mice with prostate cancer CWR22rv1 xenografts. Figure 1 shows a small-animal PET image of 2 mice 1 h after administration of ^{18}F-FPA via the tail vein. The acquisition time was 5 min. As shown in Figure 1, the CWR22rv1 tumor is clearly delineated with ^{18}F-FPA. Uptake in the tumor at 1 h after administration was 4.4 %ID/g. In addition to the tumor, the heart and brain showed high uptake. The corresponding uptake values in the heart and brain were 4.0 and 4.6 %ID/g.

Figure 2 shows small-animal PET images of mice bearing CWR22rv1 tumor xenografts, imaged with ^{18}F-FPA and ^{18}F-FDG. First, the mice were kept fasting for 4 h, and then ^{18}F-FDG was administered via the tail vein and imaged 1 h after administration. The activity was allowed to decay for 24 h, and the same mice were imaged with ^{18}F-FPA 1 h
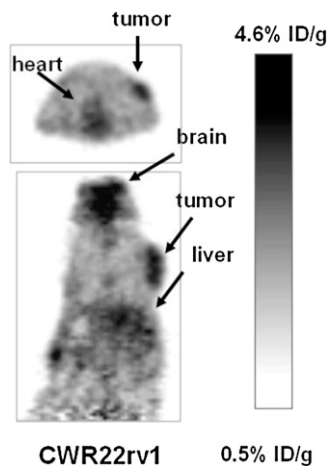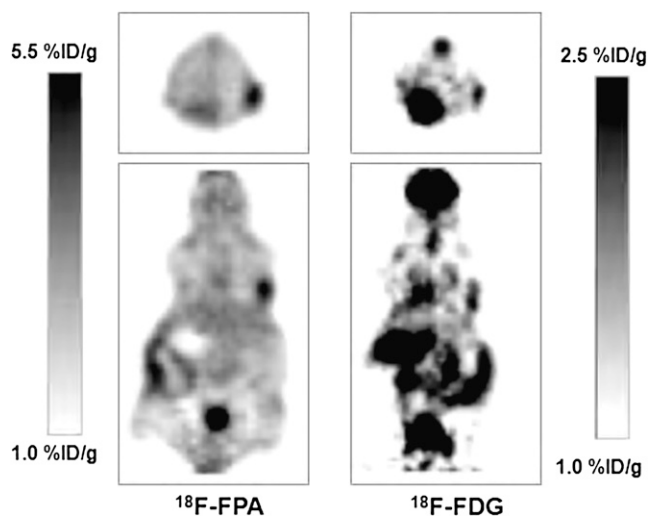

FIGURE 1. Small-animal PET images of ^{18}F-FPA in CWR22rv1 (androgen-independent) tumor–bearing mice 1 h after administration via tail vein. Images were acquired for 5 min. Tumor can easily be visualized in both transaxial and coronal slices.

after injection. In the case of ^{18}F-FPA, the animals were not fasting. As shown in Figure 2, the tumors can be readily visualized with ^{18}F-FPA, giving increased uptake and tumor contrast in comparison to ^{18}F-FDG. ^{18}F-FPA is taken up by the brain and kidneys but much less so than is ^{18}F-FDG. Figure 3 shows small-animal PET images of mice with different xenografts of prostate cancer origin. DU-145 is a cell line derived from brain metastases of prostate cancer and is androgen-independent. PC-3 is a highly metastatic androgen-independent cancer cell line derived from bone metastases. LNCaP is an androgen-sensitive cell line derived from lymph node metastases. It is apparent from PET studies that ^{18}F-FPA shows a high accumulation in various tumor xenografts, and tumors can be clearly visualized because of a high tumor-to-background ratio.

In Vivo Biodistribution

The in vivo biodistribution profile of ^{18}F-FPA at 1, 2, 3, and 4 h after administration via the tail vein in nude mice

FIGURE 2. Small-animal PET images of nude mice with CWR22 xenografts imaged with either ^{18}F-FPA or ^{18}F-FDG 1 h after tail vein injection.
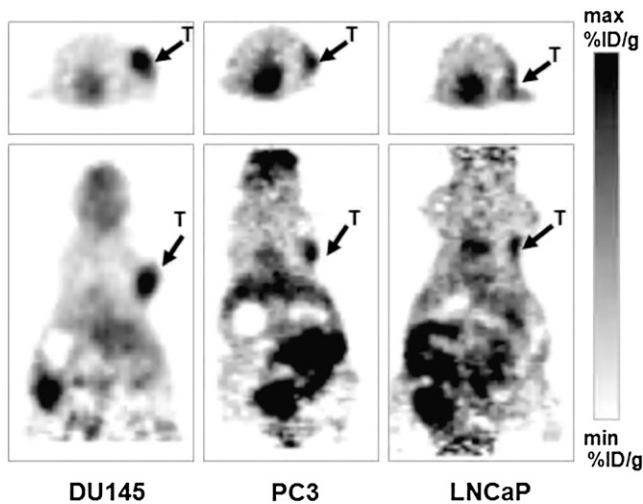
FIGURE 3. Small-animal PET images of nude mice with DU-145, PC3, and LNCaP xenografts imaged with ^{18}F-FPA 1 h after tail vein injection. Minimum and maximum values in small-animal PET images for DU-145, PC3, and LNCaP are 1.2 and 3.8, 1.5 and 3.8, and 2.0 and 4.0, respectively.

with CWR22 xenografts is shown in Figure 4. It is apparent from these data that biodistribution remains constant throughout the study. There is considerable accumulation of tracer in tumor. Tumor uptake of the tracer was 5.52 ± 0.35, 5.53 ± 0.42, 5.74 ± 0.54, and 5.34 ± 0.19 %ID/g at 1, 2, 3, and 4 h, respectively, after injection. In addition to tumor, blood and heart showed high activity. Figure 5 shows the tumor-to-organ ratio of ^{18}F-FPA at 1, 2, 3, and 4 h after injection. The tumor-to-organ ratio is greater than 1 for most of the organs with the exception of the heart, which is around 0.95.

Comparison with ^{14}C-Acetate

To compare the efficacy of ^{18}F-FPA with acetate, we performed biodistribution studies 1 h after simultaneous administration of ^{18}F-FPA and ^{14}C-acetate via the tail vein (Table 1). The %ID/g values for ^{18}F-FPA and ^{14}C-acetate in tumor were 7.08 ± 0.80 and 0.36 ± 0.08, respectively, and the corresponding tumor-to-muscle ratios were 1.94 and 2.06, respectively. Two important points to note from the data are that the %ID/g values were much higher for ^{18}F-FPA than for ^{14}C-acetate and that the ratio of this type of tumor to some organs was more favorable for ^{18}F-FPA than for ^{14}C-acetate. The biodistribution values obtained with ^{14}C acetate agreed well with ^{11}C-acetate data in the literature (5).

DISCUSSION

The suboptimal performance of ^{18}F-FDG for selective and sensitive detection of prostate tumors has spurred research in the development of alternative PET agents for detection of prostate cancers. ^{11}C-acetate was initially developed as a PET tracer to measure myocardial metabolism (17,18) but was also found to be effective in detecting prostate tumors (19). Studies on the mechanism suggest a role for fatty acid synthase, which uses acetate as its substrate for the synthesis of long-chain fatty acids. Therefore, the increased uptake of ^{11}C-acetate observed in prostate tumors has been attributed to fatty acid synthase activity (20). Despite the success of ^{11}C-acetate for diagnosing prostate tumors, the short half-life of ^{11}C is a problem for its use as a routine PET agent. In contrast, ^{18}F-labeled tracers are advantageous because their relatively long half-life (2 h) does not require an onsite cyclotron.

Long-chain carboxylic acids labeled with ^{18}F have been investigated as cardiac imaging agents for measuring myocardial uptake (21). To our knowledge, no such studies have been reported for short-chain carboxylic acids. ^{18}F-FPA was initially developed as a radioderivatization agent for labeling small peptides with ^{18}F (16). For example, the new radiotracer ^{18}F-galacto-RGD, which is currently under clinical trials for imaging $\alpha_v\beta_3$ integrin expression, uses
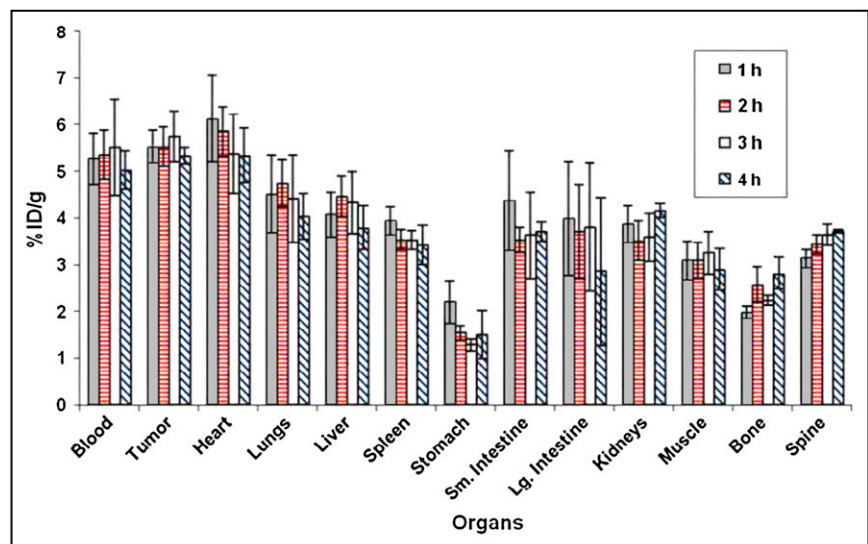
FIGURE 4. Biodistribution profile of ^{18}F-FPA in nude mice with CWR22rv1 xenografts at 1, 2, 3, and 4 h after tail vein injection. Values are mean ± SD of mean (n = 3 for each time point). Lg. = large; Sm. = small.
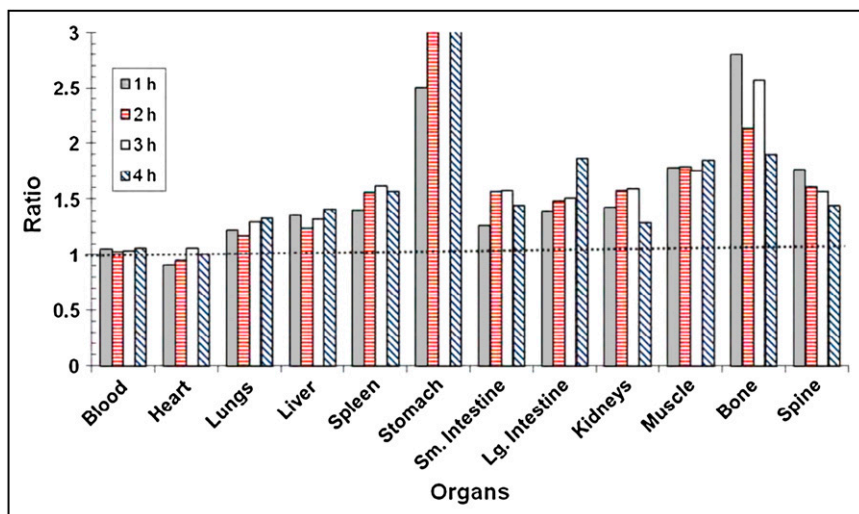
FIGURE 5. Tumor-to-organ ratio of ^{18}F-FPA in nude mice with CWR22rv1 xenografts at 1, 2, 3, and 4 h after tail vein injection. Lg. = large; Sm. = small.

^{18}F-FPA as the prosthetic group for radiolabeling the peptide (22). The biodistribution and imaging properties of ^{18}F-FPA itself have not been reported. Toxicologic studies in rats have shown that FPA caused no acute toxicity at 2.3 mmol/kg (23). Sodium, potassium, and calcium salts of propionic acid are extensively used as food additives. Metabolic studies have indicated that propionate can be used as a precursor for synthesis of fatty acids, glycogen, amino acids, and others, depending on the species (14,15,24).

^{18}F-FPA was synthesized using well-established procedures (14,15). Because the radiochemical yields obtained were high (44% ± 3% decay-corrected), further optimization of the yield was not attempted. Though the HPLC profile during sample purification indicated that the fluorination reaction was almost quantitative, the 44% overall radiochemical yield represents losses during fluoride transfers and the HPLC step. During the removal of solvent after

hydrolysis of the methyl ester, it was observed that neutralization must be performed after the removal because FPA is fairly volatile and a significant amount of compound can be lost during the process even at 45°C. In addition, during analytic HPLC, the solution must be acidic (pH < 4) because the ionized and neutral forms of FPA have fairly different retention times under the conditions used. If the pH of the injectant is greater than 4, 2 separate peaks are observed. FPA has a low molar extinction coefficient in the ultraviolet region, making accurate calculations of specific activity difficult using a standard ultraviolet detector. The specific activity calculations were based on a minimal detectable concentration of FPA. Routinely during analysis, no ultraviolet absorption peaks (mass peaks) were observed during HPLC after the purification of ^{18}F-FPA. Hence, in calculating the specific activity of ^{18}F-FPA, it was assumed the mass amount of FPA was just below the detectable limit.

TABLE 1. Comparative Biodistribution Studies of ^{18}F-FPA and ^{14}C-Acetate in Mice

Organ	%ID/g*		Tumor-to-organ ratio	
	^{18}F-FPA	^{14}C-acetate	^{18}F-FPA	^{14}C-acetate
Blood	6.88 ± 0.64	0.02 ± 0.02	1.03	16.91
Tumor[†]	7.08 ± 0.80	0.36 ± 0.08	1.00	1.00
Heart	5.46 ± 0.63	0.25 ± 0.03	1.30	1.44
Lungs	4.00 ± 0.26	0.85 ± 0.11	1.77	0.42
Liver	5.61 ± 0.50	0.67 ± 0.17	1.26	0.53
Spleen	4.36 ± 0.85	0.68 ± 0.16	1.62	0.52
Stomach	2.53 ± 1.04	0.77 ± 0.42	2.80	0.47
Small intestine	4.37 ± 1.15	0.81 ± 0.13	1.62	0.44
Large intestine	3.71 ± 1.09	0.56 ± 0.20	1.91	0.64
Kidneys	4.17 ± 0.60	0.58 ± 0.14	1.70	0.62
Muscle	3.66 ± 0.50	0.17 ± 0.03	1.94	2.06
Bone	1.68 ± 0.54	0.29 ± 0.11	4.23	1.22
Brain	5.57 ± 0.33	0.30 ± 0.02	1.27	1.17

*Mice euthanized 1 h after simultaneous administration of ^{18}F-FPA and ^{14}C-acetate via tail vein injection. Values are mean ± SD of mean (n = 4).
[†]CWR22rv1 tumors.

In vivo studies indicate that ^{18}F-FPA can successfully detect prostate tumor xenografts in mice. Biochemical studies are under way to investigate the exact mechanism of uptake of ^{18}F-FPA in prostate cancers. As shown in the PET images (Figs. 1–3) and biodistribution data (Figs. 4 and 5), the compound localizes in the tumor and is retained throughout 4 h of observation. In addition to tumor, the heart, brain, and bladder show a high amount of activity. ^{18}F-FPA primarily clears through urine, as bladder shows a high amount of activity in PET images, similar to that seen with ^{18}F-fluoroacetate or ^{18}F-fluoroethylcholine. Similar to ^{18}F-fluoroacetate, ^{18}F-FPA has a fairly constant activity in tumor, and except for bone, the tumor-to-organ ratios do not differ much at the 30-min and 2-h time points (5). Unlike ^{18}F-fluoroacetate, ^{18}F-FPA appears to show no evidence of defluorination, and both PET and biodistribution studies show low bone uptake.

At later time points, activity was localized in the lower part of the gut. This region of the intestines has been shown to be one in which absorption of small carboxylic acids occurs. In our comparative imaging study with ^{18}F-FDG, it was observed that for CWR22rv1 tumor xenografts, the smaller the tumor size was, the lower was the ^{18}F-FDG uptake (unpublished data, December 2008). However, with ^{18}F-FPA even the smaller tumors (<6 mm) were clearly delineated as shown in Figure 2.

CONCLUSION

In the present study, we have evaluated the potential of ^{18}F-FPA as a PET tracer for imaging prostate cancer. Biodistribution and PET studies indicate that ^{18}F-FPA accumulates in the tumors and produces high tumor-to-background ratios. In comparison with ^{18}F-FDG, ^{18}F-FPA shows better delineation of CWR22rv1 prostate cancer xenografts on PET studies. In addition, ^{18}F-FPA has a much higher %ID/g than does acetate. These studies support our hypothesis that ^{18}F-FPA is a promising PET tracer for prostate cancer imaging, and further studies are warranted to examine if ^{18}F-FPA offers any advantages over existing tracers for prostate cancer.

ACKNOWLEDGMENTS

REFERENCES

1. Jemal A, Siegel R, Ward E, et al. Cancer statistics, 2008. *CA Cancer J Clin.* 2008;58:71–96.
2. John SS, Zietman AL, Shipley WU, Harisinghani MG. Newer imaging modalities to assist with target localization in the radiation treatment of prostate cancer and possible lymph node metastases. *Int J Radiat Oncol Biol Phys.* 2008; 71(1, suppl)S43–S47.
3. Bouchelouche K, Oehr P. Positron emission tomography and positron emission tomography/computerized tomography of urological malignancies: an update review. *J Urol.* 2008;179:34–45.
4. Matthies A, Ezziddin S, Ulrich EM, et al. Imaging of prostate cancer metastases with ^{18}F-fluoroacetate using PET/CT. *Eur J Nucl Med Mol Imaging.* 2004;31:797.
5. Ponde DE, Dence CS, Oyama N, et al. ^{18}F-fluoroacetate: a potential acetate analog for prostate tumor imaging—in vivo evaluation of ^{18}F-fluoroacetate versus ^{11}C-acetate. *J Nucl Med.* 2007;48:420–428.
6. DeGrado TR, Coleman RE, Wang S, et al. Synthesis and evaluation of ^{18}F-labeled choline as an oncologic tracer for positron emission tomography: initial findings in prostate cancer. *Cancer Res.* 2001;61:110–117.
7. Igerc I, Kohlfurst S, Gallowitsch HJ, et al. The value of ^{18}F-choline PET/CT in patients with elevated PSA-level and negative prostate needle biopsy for localisation of prostate cancer. *Eur J Nucl Med Mol Imaging.* 2008;35:976–983.
8. Vees H, Buchegger F, Albrecht S, et al. ^{18}F-choline and/or ^{11}C-acetate positron emission tomography: detection of residual or progressive subclinical disease at very low prostate-specific antigen values (<1 ng/mL) after radical prostatectomy. *BJU Int.* 2007;99:1415–1420.
9. Kwee SA, DeGrado TR, Talbot JN, Gutman F, Coel MN. Cancer imaging with fluorine-18-labeled choline derivatives. *Semin Nucl Med.* 2007;37:420–428.
10. Veach DR, Namavari M, Pillarsetty N, et al. Synthesis and biological evaluation of a fluorine-18 derivative of dasatinib. *J Med Chem.* 2007;50:5853–5857.
11. Pillarsetty N, Cai S, Ageyeva L, Finn RD, Blasberg RG. Synthesis and evaluation of [^{18}F] labeled pyrimidine nucleosides for positron emission tomography imaging of herpes simplex virus 1 thymidine kinase gene expression. *J Med Chem.* 2006;49:5377–5381.
12. Pal A, Glekas A, Doubrovin M, et al. Molecular imaging of EGFR kinase activity in tumors with [124]I-labeled small molecular tracer and positron emission tomography. *Mol Imaging Biol.* 2006;8:262–277.
13. Veach DR, Namavari M, Beresten T, et al. Synthesis and in vitro examination of [[124]I]-, [^{125}I]- and [^{131}I]-2-(4-iodophenylamino) pyrido[2,3-d]pyrimidin-7-one radiolabeled Abl kinase inhibitors. *Nucl Med Biol.* 2005;32:313–321.
14. Lorber SH, Komarov SA, Shay H. Effect of sham feeding on gastric motor activity of the dog. *Am J Physiol.* 1950;162:447–451.
15. Pritchard GI, Tove SB. Interrelationships between the metabolism of short-chain fatty acids in ruminant liver slices. *Biochim Biophys Acta.* 1960;41:130–137.
16. Guhlke S, Coenen HH, Stocklin G. Fluoroacylation agents based on small Nca [F-18] fluorocarboxylic acids. *Appl Radiat Isot.* 1994;45:715–727.
17. Chan SY, Brunken RC, Phelps ME, Schelbert HR. Use of the metabolic tracer carbon-11-acetate for evaluation of regional myocardial perfusion. *J Nucl Med.* 1991;32:665–672.
18. Gropler RJ, Siegel BA, Geltman EM. Myocardial uptake of carbon-11-acetate as an indirect estimate of regional myocardial blood flow. *J Nucl Med.* 1991; 32:245–251.
19. Dimitrakopoulou-Strauss A, Strauss LG. PET imaging of prostate cancer with ^{11}C-acetate. *J Nucl Med.* 2003;44:556–558.
20. Vavere AL, Kridel SJ, Wheeler FB, Lewis JS. 1-^{11}C-acetate as a PET radiopharmaceutical for imaging fatty acid synthase expression in prostate cancer. *J Nucl Med.* 2008;49:327–334.
21. Knust EJ, Kupfernagel C, Stocklin G. Long-chain F-18 fatty acids for the study of regional metabolism in heart and liver: odd-even effects of metabolism in mice. *J Nucl Med.* 1979;20:1170–1175.
22. Beer AJ, Haubner R, Wolf I, et al. PET-based human dosimetry of ^{18}F-galacto-RGD, a new radiotracer for imaging alpha v beta3 expression. *J Nucl Med.* 2006;47:763–769.
23. Lock EA, Gyte A, Sturgess NC, Duffell S, Wyatt I. 2-Halopropionic acid-induced cerebellar granule cell necrosis in the rat: in vivo and in vitro studies. *Neurotoxicology.* 2001;22:363–374.
24. Buchanan JM, Hastings AB, Nesbett FB. The role of carboxyl-labeled acetic, propionic and butyric acids in liver glycogen formation. *J Biol Chem.* 1943;150:413–425.